Original Article: Efficient Removal of Cobalt(II) Ion from Aqueous Solution Using Amide-Functionalized Metal-Organic Framework

Hossein Shayegan[a] | Vahid Safarifard[a,*] | Hooman Taherkhani[b] | Mohammad Ali Rezvani[b]

[a]*Department of Chemistry, Iran University of Science and Technology, Tehran 16846-13114, Iran*
[b]*Department of Chemistry, Faculty of Science, University of Zanjan, 451561319, Zanjan, Iran*

Use your device to scan and read the article online

Citation H. Shayegan, V. Safarifard*, H. Taherkhani, M. A. Rezvani. **Efficient removal of cobalt(II) ion from aqueous solution using amide-functionalized metal-organic framework**. *J. Appl. Organomet. Chem.*, **2022**, *2*(3), 109-118.

https://doi.org/10.22034/jaoc.2022.154718

Article info:
Received: 2022-03-24
Accepted: 2022-07-07
Available Online: 2022-08-12

Checked for Plagiarism: Yes
Peer Reviewers Approved by:
Dr.SUNIL V. GAIKWAD
Editor who Approved Publication:
Professor Dr. Abdelkader Zarrouk

Keywords:
Heavy Metal Ions; Metal-Organic Frameworks; Adsorption; Langmuir; Freundlich.

ABSTRACT

In this study, an amide-functionalized metal-organic framework, namely TMU-24 was selected to adsorb Co(II) from wastewater with an adsorption capacity of 500 mg. g^{-1} in less than 20 minutes in neutral pH (pH=7). The effect of diverse parameters such as adsorbent dosage, competitive ions, and contact time on the adsorption process was investigated to find the optimal amounts of them. Also, the modeling calculations demonstrated that this compound obeys Pseudo-Second-order and Langmuir models with correlation coefficients of R^2 = 0.9996 and R^2 = 0.9761, respectively. So, the adsorption mechanism could be monolayer chemical interaction according to these models. Moreover, PXRD patterns of the framework before the adsorption procedure and after that revealed that the MOF could keep its structure, suggesting the stability of the framework. So, we can claim that our proposal adsorbent is a promising candidate for cobalt(II) removal from pollutant water.

Introduction

Heavy metal pollution is considered as a serious challenge of environmental health because of the rapid growth of industry based on its easy accumulation, toxicity, and poor degradability [1]. Since the number of radioactive wastewater increases as a result of the development of nuclear energy usage, ^{60}Co is spreading in the environment as the main component of radioactive wastes [2]. This element, which exists in the cooling water of reactors as the corrosion product, using irradiation breeding, radiotherapy and nondestructive inspection, threaten human life by some diseases including aplastic anemia, lung irritations, bone defects paralysis, diarrhea and leukemia [2-4]. Accordingly, the removal of cobalt from radioactive wastewater is required for environmental protection. For this purpose, various methods have been

*Corresponding Author: Vahid Safarifard (vsafarifard@iust.ac.ir)

mentioned in literature such as extraction, biological treatment, electrochemical ion exchange, chemical precipitation, membrane filtration, and adsorption. Among these techniques, adsorption performs as a promising separation route due to its low cost, regeneration as well as ease of operation.

Metal-organic frameworks (MOFs) are a subdivision of coordination polymers that have been developing rapidly in recent decades [5]. MOF materials are constructed from metal ions or metal ion clusters and organic bridging ligands. They exhibit many advantages containing the availability of in-pore functionality and outer-surface modification, permanent porosity [6], highly tunable structures [7], high surface areas as well as large pore volumes. Therefore, they could be helpful in a wide range of applications like drug delivery, catalysis, gas storage, electronic devices, artificial photosynthesis, detection, and adsorptive removal of hazardous substances.

Up to now, some studies have reported the Co(II) removal from wastewater *via* different MOFs including MIL-101-glycine and its two derivations, UiO-66 [3] and Fe_3O_4@SiO_2@UiO-66-Glu composite [4]. Herein, we chose amide-functionalized TMU-24, formulated as $[Zn_2(oba)_2(bpfn)]\cdot(DMF)_2$, to assess its performance in the heavy metallic pollution removal, leading to the adsorption capacity of 500 $mg.g^{-1}$ toward cobalt ions. Further investigations showed that our compound follows Pseudo-Second-order and Langmuir models with correlation coefficients of R^2=0.9996 and R^2=0.9761, respectively.

Experimental Section

Materials and methods

All utilized materials were purchased from Merk and Sigma-Aldrich companies. The infrared spectra were collected with a Nicolet 100 Fourier transform infrared (FTIR) spectrometer in the range of 400-4000 cm^{-1}. Powder X-ray diffraction (PXRD) measurements were done by using a Philips X'Pert diffractometer with a monochromated Cu Kα radiation (λ = 1.54056 Å). Inductively coupled plasma atomic emission spectrometry (ICP-AES) on a Varian Vista-PRO instrument, equipped with a charge-coupled detector, was applied to assign the remaining concentration of metal ions.

Synthesis of bpfn

1,5-Diaminonaphthalene (1.580 g; 10 mmol) was dissolved in 50 mL of dry THF containing 2.84 mL of TEA (20.4 mmol). Then, isonicotinoyl chloride hydrochloride (3.560 g, 20 mmol) was added into these solutions and heated under reflux for 24 h. The obtained suspension was filtered, dried under ambient conditions, and poured into an aqueous saturated solution of Na_2CO_3 (50 mL). The resulting white solid was finally filtered and dried and used as the MOF's pillar.

Synthesis of $[Zn_2(oba)_2(bpfn)]\cdot(DMF)_2$ (TMU-24)

Zn(*acetate*) (1 mmol) was mixed with H_2oba (0.258 g, 1 mmol), and bpfn (0.5 mmol) dissolving in DMF (50 mL) then the mixture was sonicated until all solids were dispersed uniformly and the reaction was completed (~30 min). Red-brown (TMU-24) powders were obtained as pure phases, washed by DMF, and dried at room temperature as reported in the literature previously [8]. IR (cm^{-1}): 1667 (vs), 1595 (vs), 1570 (m), 1505 (s), 1386 (vs), 1235(s), 1158 (vs), 1089 (m), 1065 (m), 1015 (m), 878 (m), 659 (m), 522 (m) (Figure 1d).

Adsorption experiments

In this study, the influence of different parameters on the absorption behavior of TMU-24 was assessed. In this way, 50 mL of cobalt solution was added to5 mg of the MOF, at room temperature and in ultrasonic baths. $Co(NO_3)_2.6H_2O$ were used as the source of cobalt ions. The solution pH was fixed by adding 0.1 mL of 0.1 M sodium hydroxide or 0.1 M HCI. Then the obtained mixture was centrifuged for 6 min. In the last step, sampling from the solution was carried out. The total amount of adsorbed heavy-metal ions on the adsorbent and the removal efficiency were

calculated using following eqs 1 and 2, respectively:

$$Q_t = \frac{(C_0 - C_t)V}{m} \quad (1)$$

$$\%R = \frac{(C_0 - C_e)}{C_0} \times 100 \quad (2)$$

Where C_0 and C_e are the initial and equilibrium concentrations of Co(II) ions (mg L^{-1}) respectively, V refers to the volume (L) of samples, and m to the adsorbent mass (g). The kinetics of the adsorption process on TMU-24 was evaluated by sampling a solution containing cobalt and adsorbent at intervals of 3-30 min. Also, absorbent isotherms were collected by adding 5 mg of adsorbent to various concentrations (5 to 125 mg L^{-1}) of Co(II).

Result and Discussion

The amide-functionalized TMU-24 crystallizes in monoclinic C2/c space group as a threefold 6-connected interpenetrated network with pcu topology (Figure 1a). The bpfn ligand has two amide groups, that each of them possess two types of donor-acceptor affinity sites: the -NH moiety that can act as an electron acceptor (Lewis acid), and the -C=O group that can act as an electron donor (Lewis base) (Figure 1b). PXRD patterns of as-prepared MOF were compared to the simulated one exhibiting the successful synthesis procedure (Figure 1c)

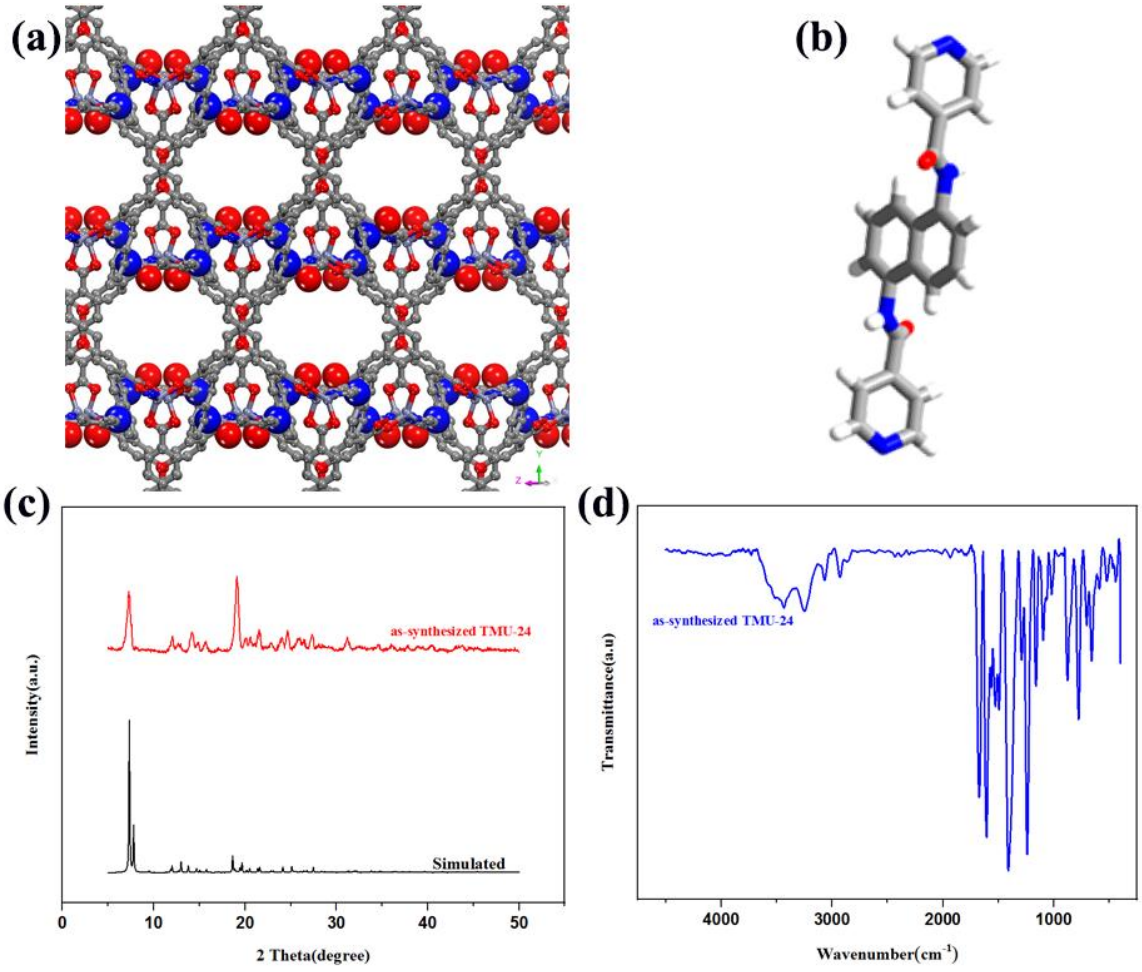

Figure 1. (a) Ball and stick representation of TMU-24. (b) Chemical structure of bpfn pillar. (c) PXRD of as-synthesized (red) and simulated (black) TMU-24. (d) FT-IR spectra of TMU-24

Adsorption tests

To confirm the most sensitivity of TMU-24 toward cobalt(II) cations, the common heavy metals including Cr^{3+}, Al^{3+}, As^{3+}, Pb^{2+}, Cu^{2+}, Ni^{2+}, Hg^{2+} as well as Co^{2+} were exposed to the MOF solution. As can be seen in Figure 2a, the proposal framework adsorbed cobalt(II) cation with the highest capacity. So the other adsorption tests were followed by this heavy metal cation.

pH is one of the most important factors in the adsorption tests which should be determined. As mentioned in literatures, in low pHs, H^+ ions compete with the analyte to gain the adsorption sites of the framework, so the adsorption capacity of the MOF toward the target analyte will decline. On the other hand, in alkali pHs, the presence of OH^- anions in the solution leads to precipitation of analyte cations, therefore the results will be incorrect. Accordingly, finding an optimum pH is necessary to continue the adsorption experiments. In this regard, the adsorption performance of TMU-24 was assessed in various pHs. As shown in Figure 2b, in neutral pH (pH=7), the most percentage of adsorption was obtained. So, this pH value was applied in the following steps.

As adsorbent dosage should be mentioned during the adsorption tests, the effect of adsorbent dosage on Co^{2+} ions adsorption capacity was examined. The optimal dosage was illustrated in Figure 2c. After that, an increase of adsorbent dosage leads to decreasing in adsorption capacity as a result of the aggregation of adsorbent and declining the ratio of adsorbing concentration to adsorbent sites.

The contact time affects the adsorption rate of the target ions too. For achieving the saturation uptake capacity, the contact time of adsorbent and adsorbate was investigated in the range of 3-30 min. As shown in Figure 2d, after 20 min contact time, the significant change in adsorption efficiency was not observed. Such fast efficiency could be as a result of the large surface area of TMU-24 and the high density of acylamide groups grafted on the MOF. Then 20 min was chosen for further investigations.

Study of sorption kinetics

To evaluate the sorption rate of Co(II) by the TMU-24, the adsorption kinetics was investigated. As demonstrated in Figure 2d, TMU-24 reaches the saturated adsorption for Co(II) (500 mg. g^{-1}) for 20 min. To find the kinetic mechanism, pseudo-first-order model and pseudo-second-order model were employed as shown as Eqs. (3) and (4), respectively [9].

$$\log(qe - qt) = \log qe - \frac{K_1}{2.303} t \quad (3)$$

$$\frac{t}{q_t} = \frac{1}{K_2 q_e^2} + \frac{t}{q_e} \quad (4)$$

where K_1 (min^{-1}) and K_2 (g/mg/min) are described as the rate constants of pseudo-first-order and pseudo-second-order adsorption, q_t (mg/g) and q_e (mg/g) point to the amount adsorbed analyte at time t (min) and the amount adsorbed at equilibrium, respectively. The kinetic plots of these models are shown in Figure 3a, b. According to the correlation coefficients of the two models, it can be concluded that the pseudo-second-order model with the higher value (=0.9996) could explain the adsorption style of Co(II) ions (Table 1). Based on this model, the adsorption process was predominantly controlled by making chemical interaction between the analyte and the active sites of TMU-24.

The Weber-Morris intraparticle diffusion model was also performed to better identify the mechanism of diffusion. The plots of Q_t versus $t^{1/2}$ in the range of the calculated adsorption lead to a nonlinear curve, which does not pass through the origin (C≠0), so the intraparticle diffusion mechanism could not participate in rate-determining step (Figure 3c).

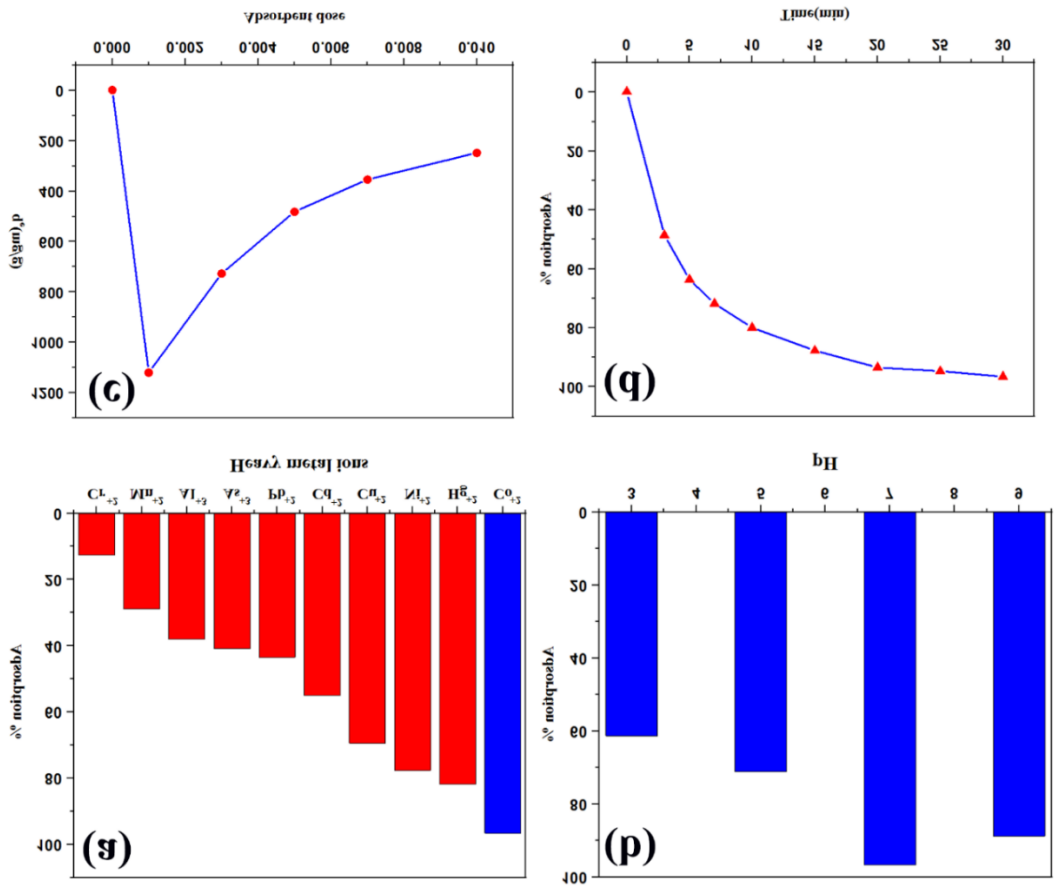

Figure 2. (a) Comparative adsorption of different heavy-metal ions. (b) pH solution effect on Co^{2+} ions adsorption efficiency for TMU-24. (c) Effect of adsorbent dosage on Co^{2+} ions adsorption capacity. (d) Effect of contact time on adsorption performance

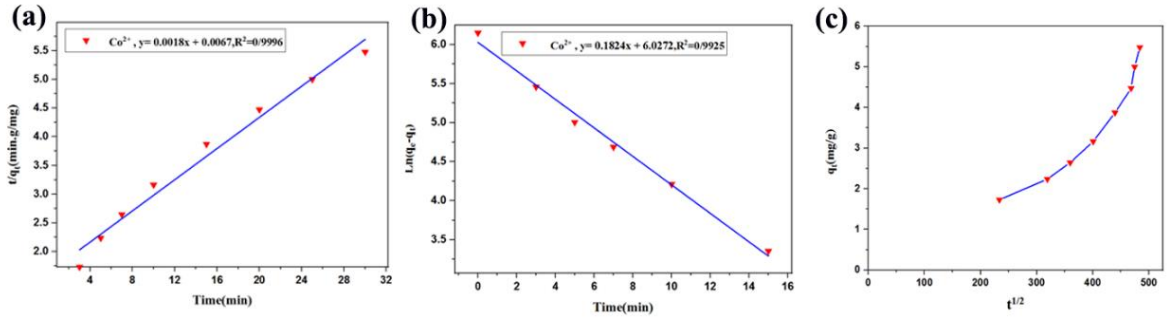

Figure 3. (a) Pseudo-second-order kinetic model. (b) Pseudo-First-order kinetic model. (c) Intraparticle diffusion kinetics model for adsorption Co^{2+} ions TMU-24

Table 1. Kinetic Sorption Parameters for Pseudo-second-order Model in Adsorption of Co^{2+} by TMU-2

Kinetic parameters			
adsorbents	**K_2(g mg $^{-1}$ min $^{-1}$)**	**Qt (mg g^{-1})**	**R^2**
TMU-24	4.84×10^{-4}	500	0.999

Adsorption isotherm

To estimate the maximal adsorption capacity as well as explore the adsorption mode of Co(II) onto TMU-24, by varying the initial Co(II) concentration (5, 10, 15, 20, 25, 50, 75, 100, and 120 ppm), the different isotherms were established and fitted using the Langmuir (5) and Freundlich (6) models as follow:

$$\frac{\mathbf{1}}{\boldsymbol{q_e}} = \frac{\mathbf{1}}{\boldsymbol{q_e}} + \frac{\mathbf{1}}{\boldsymbol{q_m}\ \boldsymbol{K_1}\ \boldsymbol{C_e}} \quad (5)$$

$$\ln q_e = ln\ K_f + \frac{1}{n} \ln C_e \quad (6)$$

where q_e is the equilibrium adsorption capacity, q_m denotes the maximum sorption capacity of the sorbent (saturation point), Ce points to the concentration of analyte ion in solution at equilibrium [mg L^{-1}] and K_l = Langmuir adsorption constant [L mg^{-1}], K_f = Freundlich isotherm constant [mgg^{-1}(L mg^{-1})$^{1/n}$] [3,10].

The Langmuir model assumes that no interaction between adsorbate molecules is formed, and the adsorption is localized in a monolayer. But in the Freundlich model, the adsorption on heterogeneous surfaces will occur. The obtained results of these two models are illustrated in Table 2 and Figure 4a,b. According to our experiments, the linear curve fits with the Langmuir model better with the higher correlation coefficient (=0.976) compared to the other one (=0.757), suggesting a monolayer adsorption mode with the maximal adsorption capacity of 500 mg. g^{-1} toward cobalt ions. Previous reports of adsorption capacity values for diverse adsorbents are compared in Table 3.

To check the reusability potential of the prepared MOF, three adsorption-desorption cycles were accomplished. Desorption was carried out through adding 2 mL of deionized water to the TMU-24@Co(II), then the solution was stirred for 20 min at ambient temperature. The amounts of total Co(II) metal ions were then determined by ICP-AES. As can be observed in Figure 4c, during three adsorption-desorption cycles, the efficiency of adsorbent decreased down to about 65% which is a satisfactory performance.

As can be seen in Figure 5a, b, the changes of SEM images of TMU-24 during adsorption confirms this adsorption type. Based on EDX spectra of TMU-24 before adsorption Co^{2+} and after that (Figure 6a,b), a new peak is appeared showing the existence of analyte on the surface of the framework confirming that the adsorption process would be carried out. Furthermore, elemental mapping of the TMU-24 emphasizes the presence of Co^{2+} in the structure after the adsorption procedure (Figure 6c,d). The similarity of the PXRD patterns of the TMU-24 before adsorption procedure and after that demonstrates the structural stability in the different steps of the Co^{2+} process (Figure 7a). Moreover, the infrared spectrum of the adsorbents was recorded before the uptake process and after that. Some slight changes in the position and shape of C-H, C=O, and C-O peaks have indicated the interaction between C-H, C=O, and C-O groups of the linkers with the Co^{2+}, which declines the frequency and energy of functional groups (Figure 7b).

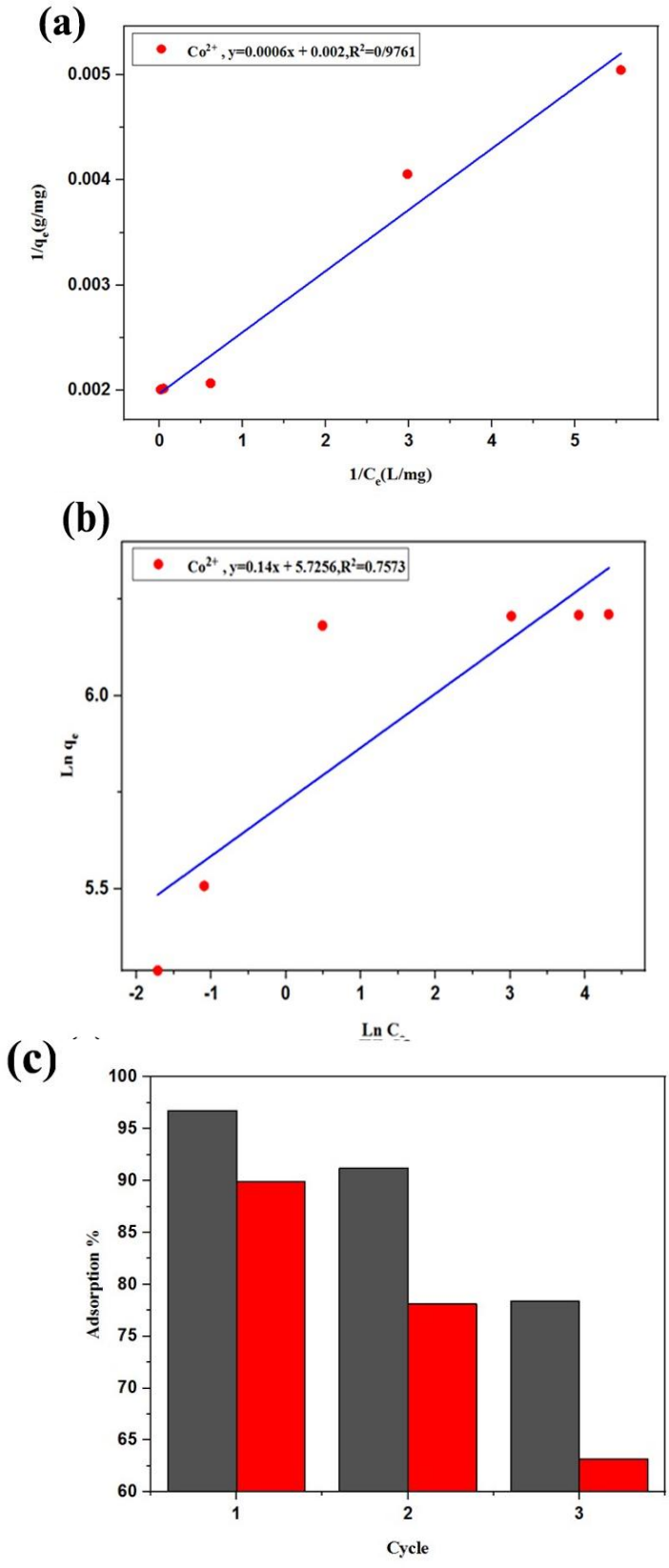

Figure 4. (a) Linear curve fitting with the Langmuir model. (b) Linear curve fitting with Freundlich model. (c) Adsorption-desorption cycles

Table 2. Langmuir and Freundlich factors for sorption of Co^{2+}

	Langmuir			Freundlich		
Adsorbents	**q_m(mg g^{-1})**	**b (L mg^{-1})**	**R^2**	**K_F**	**n**	**R^2**
TMU-24	500	3.33	0.976	135.4	5.34	0.757

Table 3. Comparison of sorption capacities of various adsorbents for Co^{2+} removal

Adsorbents	Adsorption capacities (mg g^{-1})	Time (min)	Optimal pH	Refs.
UiO-66-Schiff base	256.0	300	9	[3]
Biogenic glutamic acid-based resin	137.0	120	7	[11]
Ligand immobilized mesoporous silica	170.2	180	7	[12]
Iron/graphene composite	134.3	240	5.7	[13]
Co(II)-imprinted polymer	181.7	720	5	[14]
MIL-101-triglycine	232.6	1440	8.3	[2]
Porous resin	71	1440	5	[15]
Amination graphene oxide	116	180	7	[16]
Organicligand/mesoporous silica	205	80	8	[17]
TMU-24	500	30	7	This work

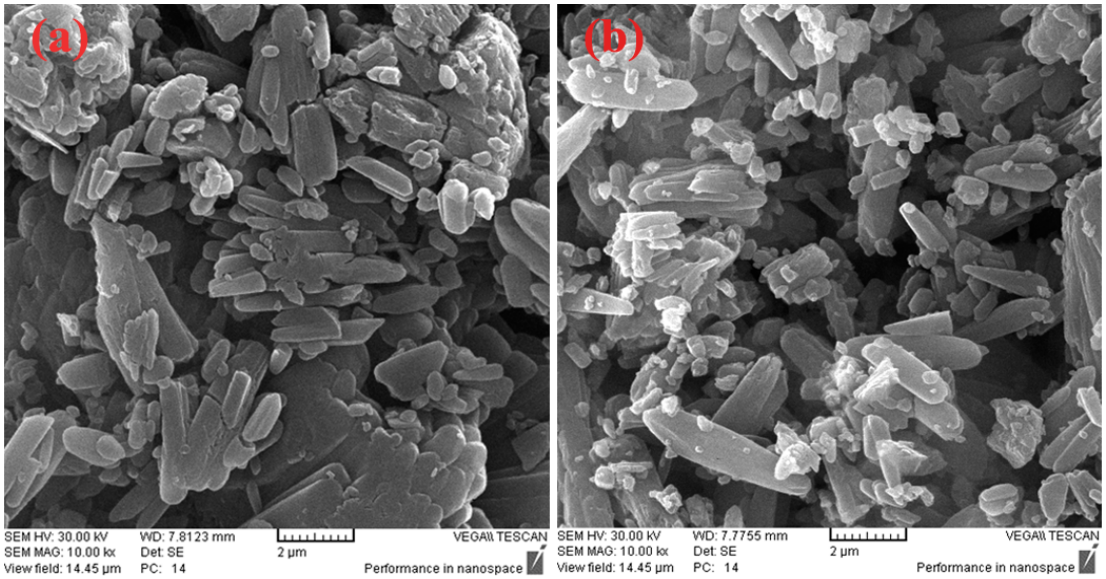

Figure 5. (a) SEM images of TMU-24 before adsorption Co^{2+}. (b) SEM images of TMU-24 after adsorption Co^{2+}

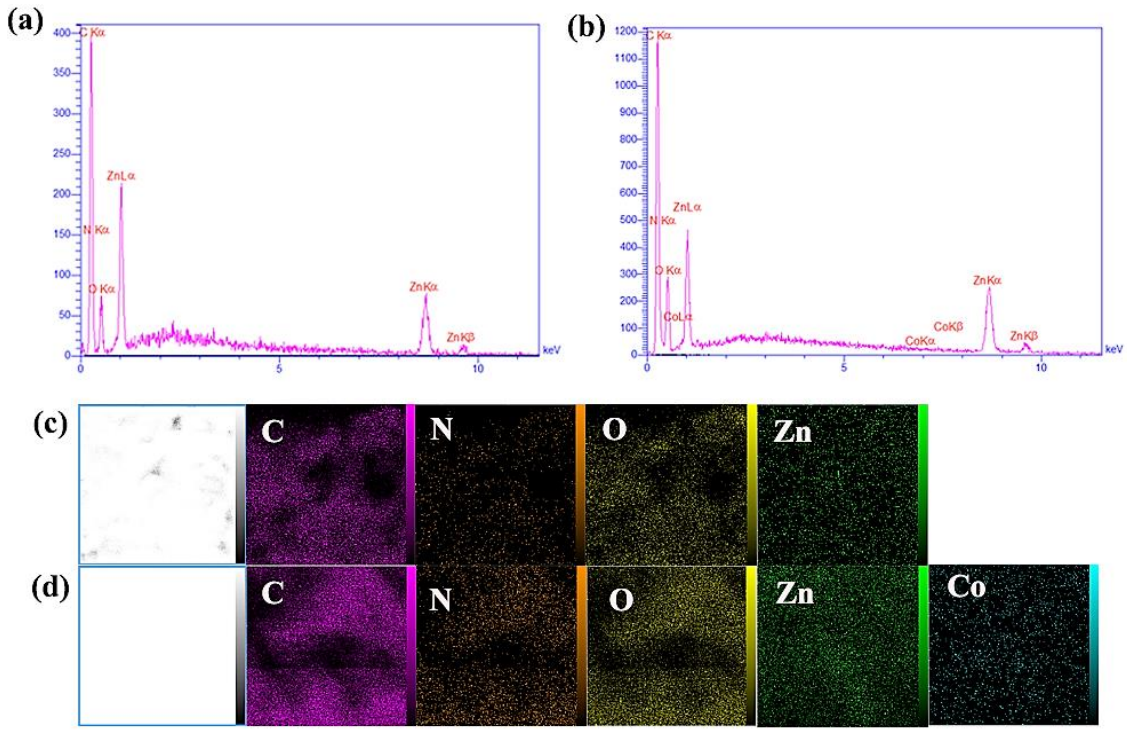

Figure 6. (a) EDX spectra of TMU-24(a) Before adsorption Co^{2+}. (b) After adsorption Co^{2+}.(c) Elemental mapping of TMU-24 before sorption process (d) Elemental mapping of TMU-24 after Co^{2+} adsorption

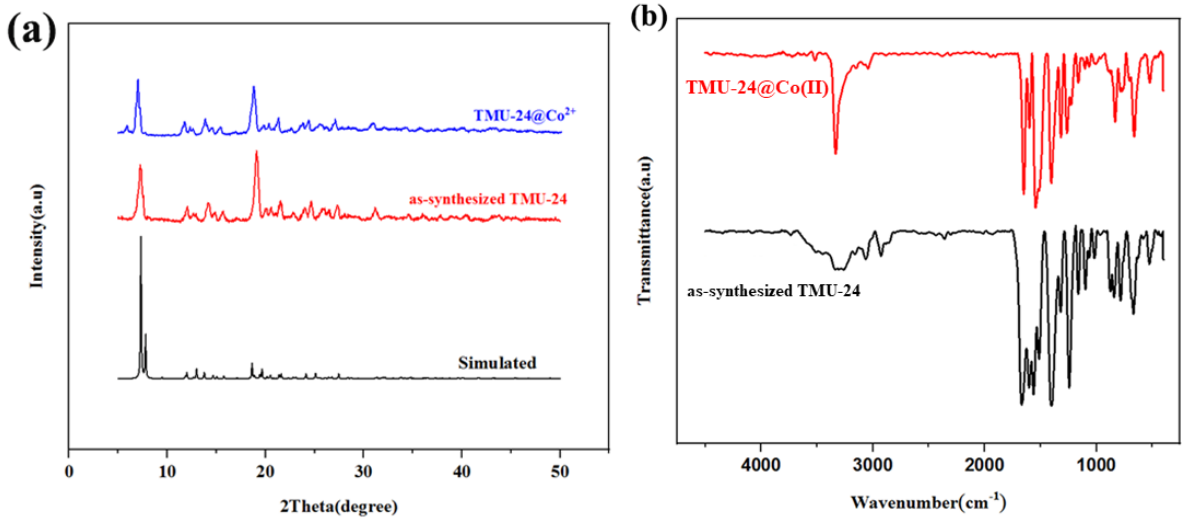

Figure 7. (a) PXRD of simulated (black), as-synthesized (red), after adsorption Co^{2+}(blue). (b) FT-IR spectra of TMU-24 as-synthesized (black) and TMU-24 after adsorption Co^{2+}(red)

Conclusion

In this work, an amide-functionalized MOF, which is called TMU-24, was obtained with H_2oba and bpfn ligands to examine its adsorption potential toward pollutant heavy metal ions. The results exhibit that TMU-24 removes Co^{2+} with higher capacity in

comparison with other metal ions. Then, the impacts of diverse factors were investigated on the adsorption performance of the MOF. The adsorption procedure was performed in less than 20 minutes. Also, by using FTIR, PXRD, EDS, and SEM images, the mechanism of sorption was understood. We indicated that the analyte was adsorbed on the surface of TMU-24 through monolayer chemical interaction based on Langmuir and Pseudo-Second-order models with correlation coefficients of R^2 = 0.9761and R^2 = 0.9996, respectively.

Acknowledgments

The financial support of this research by Iran University of Science and Technology (IUST) is gratefully acknowledged.

References

[1] Y. Fang, J. Wen, G. Zeng, F. Jia, S. Zhang, Z. Peng, H. Zhang, *Chem. Eng. J*., **2018**, *337*, 532-540. [Crossref], [Google Scholar], [Publisher]
[2] G. Yuan, H. Tu, M. Li, J. Liu, C. Zhao, J. Liao, Y. Yang, J. Yang, N. Liu, *Appl. Surf. Sci*., **2019**, *466*, 903-910. [Crossref], [Google Scholar], [Publisher]
[3] G. Yuan, Y. Tian, J. Liu, H. Tu, J. Liao, J. Yang, Y. Yang, D. Wang, N. Liu, *Chem. Eng. J.,* **2017**, *326*, 691-699. [Crossref], [Google Scholar], [Publisher]
[4] G. Yuan, C. Zhao, H. Tu, M. Li, J. Liu, J. Liao, Y. Yang, J. Yang, N. Liu, *Inorg. Chim. Acta,* **2018**, *483*, 488-495. [Crossref], [Google Scholar], [Publisher]
[5] L. Fu, S. Wang, G. Lin, L. Zhang, Q. Liu, J. Fang, C. Wei, G. Liu, *J. hazard. Mater.,* **2019**, *368*, 42-51. [Crossref], [Google Scholar], [Publisher]
[6] L. Liang, L. Liu, F. Jiang, C. Liu, D. Yuan, Q. Chen, D. Wu, H.-L. Jiang, M. Hong, *Inorg. Chem.,* **2018**, *57*, 4891-4897. [Crossref], [Google Scholar], [Publisher]
[7] T. He, Y.-Z. Zhang, X.-J. Kong, J. Yu, X.-L. Lv, Y. Wu, Z.-J. Guo, J.-R. Li, *ACS Appl. Mater. Interfaces,* **2018**, *10*, 16650-16659. [Crossref], [Google Scholar], [Publisher]
[8] V. Safarifard, S. Rodríguez-Hermida, V. Guillerm, I. Imaz, M. Bigdeli, A. Azhdari Tehrani, J. Juanhuix, A. Morsali, M. E. Casco, J. Silvestre-Albero, *Cryst. Growth Des.,* **2016**, *16*, 6016-6023. [Crossref], [Google Scholar], [Publisher]
[9] Y. Wu, G. Xu, F. Wei, Q. Song, T. Tang, X. Wang, Q. Hu, *Micropor. Mesopor. Mater.,* **2016**, *235*, 204-210. [Crossref], [Google Scholar], [Publisher]
[10] J. E. Efome, D. Rana, T. Matsuura, C.Q. Lan, *J. Mater. Chem. A,* **2018**, *6*, 4550-4555. [Crossref], [Google Scholar], [Publisher]
[11] Z.A. Jamiu, T.A. Saleh, S.A. Ali, *J. hazard. Mater.,* **2017**, *327*, 44-54. [Crossref], [Google Scholar], [Publisher]
[12] M.R. Awual, N.H. Alharthi, M.M. Hasan, M.R. Karim, A. Islam, H. Znad, M.A. Hossain, M.E. Halim, M.M. Rahman, M.A. Khaleque, *Chem. Eng. J.*, **2017**, *324*, 130-139. [Crossref], [Google Scholar], [Publisher]
[13] M. Xing, J. Wang, *J. Colloid Interface Sci.,* **2016**, *474*, 119-128. [Crossref], [Google Scholar], [Publisher]
[14] W. Guo, R. Chen, Y. Liu, M. Meng, X. Meng, Z. Hu, Z. Song, *Colloid Surface A,* **2013**, *436*, 693-703. [Crossref], [Google Scholar], [Publisher]
[15] M. Cegłowski, G. Schroeder, *Chem. Eng. J.*, **2015**, *263*, 402-411. [Crossref], [Google Scholar], [Publisher]
[16] F. Fang, L. Kong, J. Huang, S. Wu, K. Zhang, X. Wang, B. Sun, Z. Jin, J. Wang, X.-J. Huang, *J. hazard. Mater.,* **2014**, *270*, 1-10. [Crossref], [Google Scholar], [Publisher]
[17] M.R. Awual, T. Yaita, Y. Okamoto, *Sensor. Actuat. B- Chem.,* **2014**, *203*, 71-80. [Crossref], [Google Scholar], [Publisher]